Two-Port Noise and Impedance Measurements for Two-Terminal Devices with a Resonant Tunneling Diode Example

Andreas Przadka, Kevin J. Webb, *Senior Member, IEEE,* and David B. Janes, *Member, IEEE*

***Abstract*— A two-port technique is presented for determining the circuit elements and noise sources of the equivalent circuit of a two-terminal device at microwave frequencies. The two-terminal device is connected as a two-port so that intrinsic and parasitic circuit elements can be obtained from full two-port S-parameter measurements. This measurement does not require one of the two contacts to be grounded, which makes it particularly well suited for the characterization of integrated devices where parasitic elements become important and cannot be easily calculated. The noise of the device is measured by employing a noise-figure meter and the intrinsic noise is computed from the measured terminal noise. As an example, the impedance and noise elements of a resonant tunneling diode (RTD) are measured over frequency ranges of 2–8 and 2–4 GHz, respectively.**

***Index Terms*— Equivalent circuits, impedance measurement, noise, noise measurement, one-port circuits, resonant tunneling diodes.**

I. Introduction

TWO-TERMINAL semiconductor devices, commonly termed one-ports, are of considerable interest for a variety of high-speed applications such as mixers and detectors. For each given stage of device technology, two-terminal devices (e.g., diodes) operate at higher frequencies than corresponding three-terminal devices (transistors), which are typically operated as two-ports, due to their simplified structure. Particular examples for such devices are Schottky diodes [1] and resonant tunneling diodes (RTD's) [2]. These two-terminal devices can be described with the equivalent circuit shown in Fig. 1(a). It consists of the impedance elements R_S, $R_D(V)$, and $C_D(V)$, and the noise sources $\overline{v_S^2}$ and $\overline{i_D^2(V)}$, which are taken to be independent of frequency. Because of the general nature of the equivalent-circuit model used, our approach can be applied to a wide class of high-frequency devices.

A particular difficulty for noise measurements on two-terminal devices is that most commercial equipment for noise measurements, in particular, the noise-figure meter,[1] is designed for two-ports that have gain. Two-terminal devices do not have gain unless they have negative differential resistance (NDR) and are biased in that region. The error for the noise measurement is, therefore, expected to be high because the noise of the measurement system contributes significantly to the overall measured noise power [3].[2] Additionally, the intrinsic noise, i.e., $\overline{i_D^2}$, is very sensitive to errors in the equivalent-circuit elements R_S, $R_D(V)$, and $C_D(V)$, which must be determined accurately.

The common approach to measure noise of two-terminal devices with a noise-figure meter is the reflection arrangement [3]–[6]. Impedance elements are found by measuring the reflection coefficient or can even be computed from the device structure and the dc–IV curve [7]. This does require one of the terminals to be grounded, which is easily achieved for discrete devices with one contact on the backside of the wafer.

On the other hand, integratable devices have both contacts on the top side of the wafer [8] and a ground plane at the back of the wafer, which represents an independent third terminal, introducing additional parasitics. Also, it is not an easy task to ground one of the top contacts without introducing additional parasitics.

For noise and impedance measurements, we, therefore, propose connecting the two-terminal device as a two-port, each contact being one of the ports with respect to ground, as shown in Fig. 1(b). The additional information obtained from a full two-port measurement, in contrast to a reflection measurement, makes it possible to determine the elements of a more complicated equivalent circuit and, therefore, to correctly account for the parasitic elements inherent in the integrated device structure. The impedance Z_D represents the effect of R_S, $R_D(V)$, and $C_D(V)$. The two internal noise sources $\overline{i_D^2}$ and $\overline{v_S^2}$ are mapped to the input and combined into one $\overline{v_n^2}$. This configuration has the advantage that full two-port S-parameter measurements can be performed, none of the contacts need to be grounded, and the same packaging is used for all measurements.

II. Impedance Measurement

We assume that full two-port S-parameters are measured with the device mounted in a fixture and connected by bond wires/ribbons. In order to describe the parasitic effects of the bond wires/ribbons and pad capacitances, we add a shunt

Manuscript received June 6, 1997; revised May 8, 1998. This work was supported by the National Science Foundation under Grant DMR-9 400 415.

The authors are with the School of Electrical and Computer Engineering, Purdue University, West Lafayette, IN 47907-1285 USA.

Publisher Item Identifier S 0018-9480(98)06142-0.

[1] *Fundamentals of RF and Microwave Noise Figure Measurements,* Hewlett-Packard Applicat. Note 57-1, Santa Rosa, CA 1983.

[2] *Noise Figure Measurement Accuracy,* Hewlett-Packard Applicat. Note 57-2, Santa Rosa, CA 1983.

capacitance C_1 and C_2 to ground and a series inductor L_1 and L_2 to each port of the equivalent-circuit model.

The packaged device, including the effects of the fixture, will be referred to as the device-under-test (DUT). The part of the device that can be described by the R_D–C_D parallel circuit will be denoted as the intrinsic device. The device with R_S, $C_{1/2}$, and $L_{1/2}$ included will be called the extrinsic device. In order to determine the S-parameters of the extrinsic device, a deembedding scheme such as the through-reflect line (TRL) method [9] can be used.

Since the network analyzer is calibrated, using coaxial standards, before measuring the calibration standards for the fixture, we can also compute the S-parameters of each fixture half itself by extending the treatment in [9]. This data will be needed for the noise deembedding.

The elements of the equivalent circuit were determined from the measured and deembedded S-parameters of the extrinsic device.

First, L_1 and L_2 were determined from a least mean square (LMS) fit to the S-parameters for zero bias and the upper half (4–8 GHz) of the measurement band, where the sensitivity for finding L_1 and L_2 is largest. Their effect was then removed from the measured S-parameters for each bias point by appropriate matrix manipulations [10] and the remaining data were expressed as $ABCD$-parameters. The remaining equivalent circuit has the pi-topology, consisting of the shunt elements $Y_1 = j\omega C_1$ and $Y_2 = j\omega C_2$ and the series element Y_3. From the $ABCD$-parameters of the pi-equivalent circuit, we can now identify $Y_1 = (D-1)/B$, $Y_2 = (A-1)/B$, and $Y_3 = 1/B$.

The parasitic capacitances are obtained from the slope of the plot of the shunt admittances (Y_1 and Y_2) versus frequency, which are ideally straight lines through the origin. The values for R_S, $R_D(V)$, and $C_D(V)$ were obtained from Y_3. First, an LMS fit with R_S, $R_D(0)$, and $C_D(0)$ as parameters was performed for zero bias when $Y_3 \approx R_S + (1/j\omega C_D)$ so that we have good sensitivity for finding R_S and C_D.

The bias-dependent elements R_D and C_D were then computed from Y_3 at each bias point by first removing the series resistance, which results in the admittance of the intrinsic device $Y_3' = (1/(1/Y_3) - R_S)$. For each frequency, R_D and C_D can now be found by recognizing that $R_D = (1/\mathrm{Re}\{Y_3'\})$ and $f \times C_D = (\mathrm{Im}\{Y_3'\}/2\pi)$. R_D was determined by forming the average over frequency and C_D by fitting a straight line through the origin to $(\mathrm{Im}\{Y_3'\}/2\pi)$ and reading of the slope. This procedure can also be used to establish error bounds ΔC_D and ΔR_D by demanding that the true value must lie within the standard deviation of the fit.

At this point, all the equivalent-circuit elements L_1, L_2, C_1, C_2, R_S, $R_D(V)$, and $C_D(V)$ have been determined.

III. Noise Measurement

For the noise measurements we use a noise-figure meter.[1] Because the noise figure and noise-figure meter are two-port concepts, the two-terminal device needs to be connected in a two-port configuration. With our particular arrangement the measured noise figure F of the resulting two-port can be used to extract the noise temperature of the corresponding two-terminal device T_n with

$$T_n = (F_a - 1)\frac{T_0 Z_0}{\mathrm{Re}\{Z_D\}}. \tag{1}$$

Z_D is the impedance of the two-terminal device, Z_0 the impedance of the noise source used for the noise-figure measurement, and $T_0 = 290$ K the reference temperature. The noise temperature T_n uniquely specifies the noise of the two-terminal device and is not dependent on the connection arrangement. T_n is related to the effective source voltage variance by $\overline{v_n^2} = 4kT_nB\,\mathrm{Re}\{Z_D\}$ with k being the Boltzmann's constant and B the measurement band width.

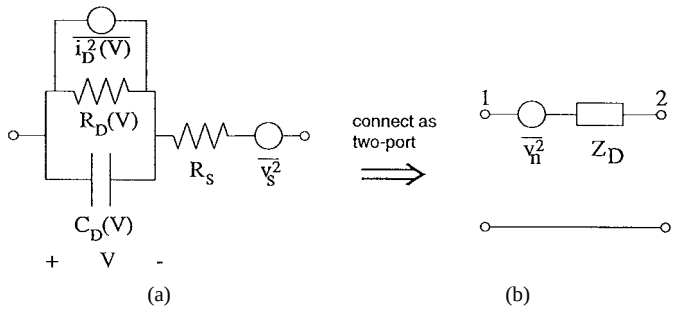

Fig. 1. (a) Equivalent-circuit model for a two-terminal device. R_S is the series resistance, $R_D(V)$ and $C_D(V)$ are bias dependent and represent the intrinsic device. The noise sources $\overline{v_S^2}$ and $\overline{i_D^2(V)}$ describe the thermal noise of R_S and the thermal and bias driven noise of the intrinsic device, respectively. (b) Two-terminal device connected as two-port.

Our goal is to determine the noise sources $\overline{i_D^2(V)}$ and $\overline{v_S^2}$ in the generic equivalent circuit of the two-terminal device [shown in Fig. 1(a)]. The value for the two noise sources can be determined from the measured noise figure of the extrinsic device F_D which, in turn, can be computed from the noise figure of the DUT F_{DUT} using the Friis relation for three cascaded elements

$$F_{\mathrm{DUT}} = F_{\mathrm{fix1}} + \frac{F_D - 1}{G_{\mathrm{fix1}}} + \frac{F_{\mathrm{fix2}} - 1}{G_{\mathrm{fix1}} G_D}. \tag{2}$$

In order to measure F_{DUT}, two noise measurements are needed, one calibration measurement and the actual measurement with the DUT inserted into the measurement system, resulting in F_{CAL} and F_{MES}, respectively. The arrangement for the actual measurements is shown in Fig. 2. For the calibration measurement, an adapter is inserted in place of the DUT which, in our case, was a male–male barrel. In order to distinguish the variables of the calibration measurement, we use the subscript CAL wherever MES appears. The noise figure and available gain of the adapter are called F_{adap} and G_{adap}, respectively. The reflection coefficient looking into the right port of the adapter will be called Γ_S'', and the noise figure of the noise-measurement system (nms) with the adapter included will be called $F'_{\mathrm{nms,CAL}}$.

The measured noise figure during the calibration measurement F_{CAL} includes the noise of the measurement system and the circuit components needed to connect and bias the DUT. We can write

$$F_{\mathrm{CAL}} = F_{\mathrm{loss}} + \frac{F_{\mathrm{adap}} - 1}{G_{\mathrm{loss}}} + \frac{F_{\mathrm{load,CAL}} - 1}{G_{\mathrm{adap}} G_{\mathrm{loss}}}$$

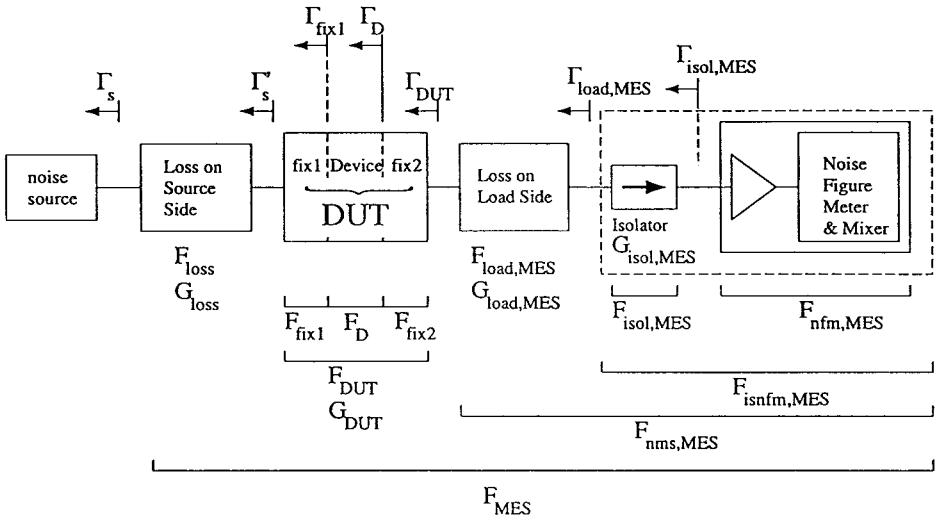

Fig. 2. Noise-measurement setup for the measurement step when the packaged device is inserted.

$$+\frac{F_{\mathrm{isol,CAL}}-1}{G_{\mathrm{adap}}G_{\mathrm{loss}}G_{\mathrm{load,CAL}}} +\frac{F_{nfm,\mathrm{CAL}}-1}{G_{\mathrm{adap}}G_{\mathrm{loss}}G_{\mathrm{load,CAL}}G_{\mathrm{isol,CAL}}}. \quad (3)$$

For the measurement step in Fig. 2, we find, accordingly,

$$F_{\mathrm{MES}}=F_{\mathrm{loss}}+\frac{F_{\mathrm{DUT}}-1}{G_{\mathrm{loss}}}+\frac{F_{\mathrm{load,DUT}}-1}{G_{\mathrm{DUT}}G_{\mathrm{loss}}} +\frac{F_{\mathrm{isol,DUT}}-1}{G_{\mathrm{DUT}}G_{\mathrm{loss}}G_{\mathrm{load,DUT}}} +\frac{F_{nfm,\mathrm{DUT}}-1}{G_{\mathrm{DUT}}G_{\mathrm{loss}}G_{\mathrm{load,DUT}}G_{\mathrm{isol,DUT}}}. \quad (4)$$

The noise figures of the passive components on the source and load side of the DUT can be determined from their available gain [11]

$$F_{i,j}=1+\left(\frac{1}{G_{i,j}}-1\right)\frac{T}{T_0} \quad (5)$$

where T is the physical temperature of the passive two-port. The available gain is found from measured S-parameters, taking the reflection coefficient presented to the left-hand side of the corresponding two port into account. F_{loss} and G_{loss} can be considered constants for a given frequency because the influence of the differing source reflection coefficient on the final result was found to be negligible. This was verified by measuring $(\Gamma_S)_{\mathrm{cold}}$ and $(\Gamma_S)_{\mathrm{hot}}$ and doing all calculations with one and then the other.

For our measurement setup, the reflection coefficient seen by the nms changes from Γ_S'' during the calibration to Γ_{DUT} during the measurement with the DUT in place. Γ_S'' and Γ_{DUT} can be substantially different depending on the applied bias to the device. The difference will be biggest when the device is at zero bias because the two-terminal device then has a high impedance, which leads to a large $|\Gamma_{\mathrm{DUT}}|$, whereas $|\Gamma_s''|$ is essentially zero for a well-matched system. Therefore, the noise figure of the nms $F_{nms,j}$ will be different for the calibration and measurement. The nms contains an isolator at the input of the noise-figure meter (the mixer and preamplifier are considered part of the noise-figure meter for this discussion) so that the reflection coefficient seen by the noise-figure meter is the same for the calibration and the measurement, assuming that the isolator has infinite isolation. Therefore, the noise figure of the noise-figure meter is approximately the same for the calibration and measurement

$$F_{nfm,\mathrm{MES}}\approx F_{nfm,\mathrm{CAL}}. \quad (6)$$

We neglect the error that results from this approximation. However, the isolator does contribute to the noise figure of the nms because it has nonzero loss, i.e., $|S_{21,\mathrm{isol}}|<1$. In order to take the loss of the isolator into account, we simply compute its available gain $G_{\mathrm{isol,CAL}}$ and $G_{\mathrm{isol,MES}}$ and noise figure $F_{\mathrm{isol,CAL}}$ and $F_{\mathrm{isol,MES}}$ with (5). For an ideal isolator, this procedure becomes equivalent to the use of $F=(F(0)/(1-|\Gamma|^2))$ [12], where Γ is the reflection coefficient seen at the input of isolator and $F(0)$ is the noise figure of the system to the right of the isolator for $|\Gamma|=0$. With F_{CAL} and F_{MES} known from the noise measurements and $G_{\mathrm{loss,CAL/MES}}$, G_{adap}, G_{DUT}, $G_{\mathrm{load,CAL/MES}}$, Γ_S', Γ_S'', Γ_{DUT}, and $\Gamma_{\mathrm{load,CAL/MES}}$ computed from measured S-parameters, we can find F_{DUT} with the help of (3) and (4).

The S-parameters of the two fixture halves are known from the TRL deembedding, as are the S-parameters of the DUT and the extrinsic device. The noise figure of the extrinsic device F_D is now obtained from F_{DUT} by use of (5) and (2). The effect of the parasitic networks $L_{1/2}$ and $C_{1/2}$ can be removed with a formula similar to (2) by considering the parasitic networks as two-ports, resulting in F_D', which is the intrinsic noise figure plus that due to R_S.

For the intrinsic noise current $\overline{i_D^2}$ and the circuit in Fig. 1, we find under use of (1)

$$\overline{i_D^2}=\frac{4k(F_D'-1)T_0Z_0'B-4kTR_SB}{R_D^2}\left(1+\omega^2R_D^2C_D^2\right) \quad (7)$$

where Z_0' is the impedance looking through the parasitics network into fixture half one. For frequencies where $\omega^2R_D^2C_D^2\ll 1$, (7) shows the high sensitivity of $\overline{i_D^2}$ with respect to error

in R_D. We compute the noise-current variance for every frequency at which a noise measurement was performed (2–4 GHz in 0.1-GHz steps). Since these frequencies are low compared to those where the shot noise is expected to become frequency dependent, we average the data for the noise-current variance over frequency for each bias point.

The two most important error sources in $\overline{i_D^2}$ are the relative instrument error $E = (\Delta F_m/F_m)$ where F_m is the measured uncorrected noise figure, and the errors in the intrinsic circuit elements ΔR_D and ΔC_D. The E results in an error in $F_{\rm DUT}$, $\Delta F_{\rm DUT}$, computed by

$$\Delta F_{\rm DUT} = \left((G_{a,\rm load} F_{\rm MES} E)^2 + \left(\frac{G_{a,\rm load} F_{\rm CAL} E}{1 - |\Gamma_{\rm DUT}|^2} G_{a,\rm DUT} \right)^2 \right)^{1/2}. \quad (8)$$

Equation (8) can be derived by solving (2), (4), and (6) for $F_{\rm DUT}$, taking partial derivatives with respect to $F_{\rm CAL}$ and $F_{\rm MES}$, and taking the square root of the sum of the squares of the respective contributions. The resulting error in $\overline{i_D^2}$, $\Delta\overline{i_{D,F_m}^2}$ was computed by determining $\overline{i_D^2}$ for various values of $F_{\rm DUT}$ allowed by (8), using (2) and (7). The error E is due to the nonlinearity of the power detector in the noise-figure meter and is specified to be 0.25 dB for the instrument used in our measurement.[3] However, the error actually made during our measurements was found to be around 0.08 dB by measuring the noise figure of a passive two-port (DUT without bias) and comparing this to the expected result, which was computed from measured S-parameters.

The error due to the uncertainty in the circuit elements, $\Delta\overline{i_{D,R_D/C_D}^2}$ was determined by computing $\overline{i_D^2}$ from $F_{\rm DUT}$, again using (2) and (7), for various values of R_D and C_D allowed by the error bounds ΔR_D and ΔC_D, selecting the worst case. The total error $\Delta\overline{i_D^2}$ is then found from the square root of the sum of the squares of $\Delta\overline{i_{D,R_D/C_D}^2}$ and $\Delta\overline{i_{D,F_m}^2}$ from which the relative error is readily computed.

The error due to the uncertainty in the parasitics $C_{1,2}$ and $L_{1,2}$ was not included, as was not the uncertainty in determining the S-parameters and the nonrepeatability of the coaxial connections and ribbon bonds. All these error sources are negligeable in comparison to the error sources considered above.

IV. Example: The RTD

In order to demonstrate the developed measurement technique, it has been applied to an integratable RTD to find intrinsic noise results at microwave frequencies. Details of the device structure used for our measurements can be found in [13]. Two nominally identical devices, called device A and B, were investigated.

For microwave measurements, the device was mounted into a two-port test fixture comprised of a central carrier on which the device was mounted, two fixture halves with microstrip lines on alumina substrates to which the device was bonded, and coaxial K-connector launchers. Connection to the microstrip lines in each fixture half was made by ribbon bonds to reduce the parasitic inductance. S-parameter measurements were performed with an HP8510B network analyzer over a frequency range of 0.5-8 GHz. The TRL "through" was realized by connecting the fixture halves directly together and bonding the microstrip lines together. The "line" segment was a 2.4-mm piece of microstrip line mounted on a sample holder of corresponding width, again using ribbon bonding for all connections. For the "reflect," an unused sample holder was placed into the fixture and a bond connection made.

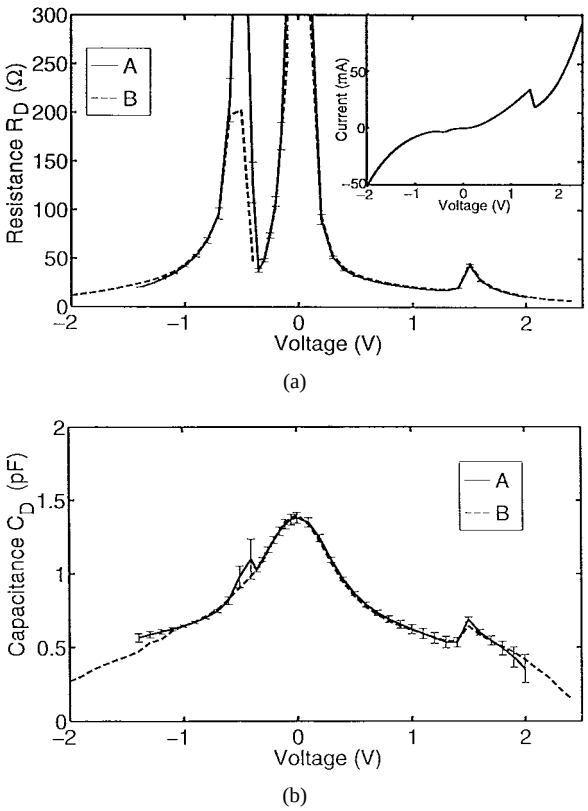

Fig. 3. The bias-dependent equivalent-circuit elements R_D and C_D plotted versus the applied voltage for forward and reverse bias. For device A, the error bars due to the fitting procedure are shown as well. The insert shows the IV curve of device A. The one for device B is nearly identical to the one shown. No values for R_D and C_D where extracted in the NDR region because the device could not be stably biased in that region.

The values obtained for the series inductors from the best fit of the S-parameters at zero bias were $L_1 = 0.435$ nH, $L_2 = 0.154$ nH for device A, and $L_1 = 0.122$ nH, $L_2 = 0.419$ nH for device B. Given the mounting arrangement of our samples, the sum of the lengths of the two bond wires and, therefore, $L_1 + L_2$ is about the same for each of the two devices. The values obtained for the parasitic capacitances were $C_1 = 0.0427$ pF and $C_2 = 0.0491$ pF for device A, and $C_1 = 0.0418$ pF and $C_2 = 0.0327$ pF for device B. All these capacitances are comparable to within 20%, which is consistent with the picture that these are mainly the capacitances between the pad metal and the grounded backside of the wafer. The series resistance we found was $R_S = 7.5\ \Omega$ and $R_S = 8.3\ \Omega$ for device A and B, respectively. The final results for $C_D(V)$ and $R_D(V)$, together with the error bars

[3] Hewlett-Packard, *Operating Manual, Noise Figure Measurement Operation for the HP8970B, HP8971B and HP8971C*, Santa Rosa, CA, 1990.

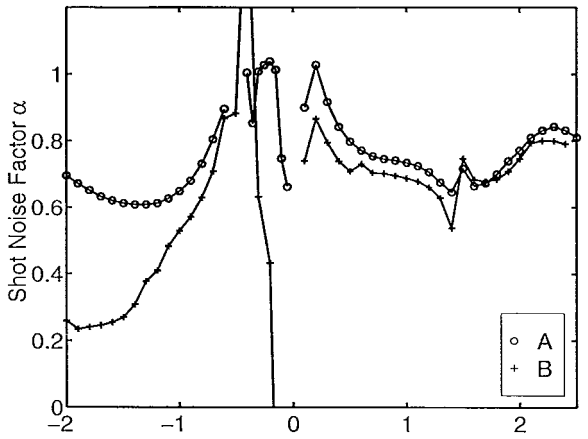

Fig. 4. Shot noise factor α as a function of applied bias for device A and B. Shot noise suppression, i.e., $\alpha < 1$, is observed for forward and reverse bias.

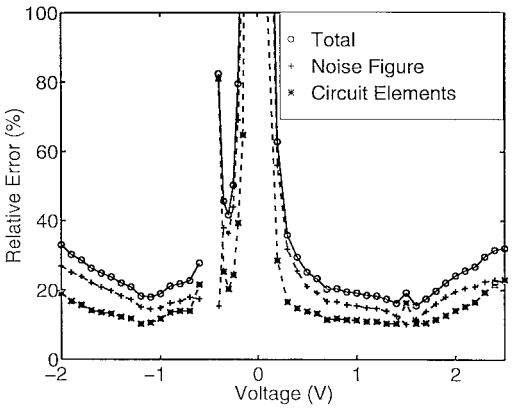

Fig. 5. Relative error in shot noise factor for device A. Also shown are the separate contributions due to the error in the noise measurement $\Delta\overline{i^2_{D,F_m}}$ and the circuit elements $\Delta\overline{i^2_{D,R_D/C_D}}$. The former is the dominating error source because preamplifier noise is high, but the latter plays an important role and will dominate for a preamplifier with very low noise.

for device A, are shown in Fig. 3. A more detailed discussion of these results can be found in [13]. No measurement of the intrinsic-circuit elements in the NDR region was attempted because the device could not be stably biased.

For the noise measurements a noise-figure meter (HP8970B) with a diode noise source (HP346C) and an additional mixer/preamplifier (the HP8971, which we refer to as a mixer) were used, allowing for a maximum measurement frequency of 26.5 GHz. A high electron-mobility transistor (HEMT) amplifier, with a noise figure of about 2.8 dB in a 50-Ω system, was placed at the input of the mixer to reduce the overall noise figure of the measurement system.

Measurements were performed for frequencies from 2 to 4 GHz in 100-MHz steps, where the frequency range was limited by the isolator used. The calibration measurement with the adaptor was repeated after having measured all bias points in order to check eventual drift in the noise figure of the measurement system. This drift was found to be negligible for the duration of our calibration cycle of about 2 h.

The noise results are shown in Fig. 4. We plot the shot noise-suppression factor α $(= \overline{i^2_D}/(2eIB)$, where e is the elctron charge and I is the dc bias current), which was averaged over the frequency range of 2–4 GHz. A physical explanation of the result is presented in [13].

Fig. 5 shows the relative error for α $((\Delta\alpha/\alpha) = (\Delta\overline{i^2_D}/\overline{i^2_D}))$ obtained from the measurements on device A, as well as the error components due to $\Delta\overline{i^2_{D,F_m}}$ and $\Delta\overline{i^2_{D,R_D/C_D}}$. The $\Delta\overline{i^2_{D,F_m}}$ is the dominant term, but $\Delta\overline{i^2_{D,R_D/C_D}}$ is significant and cannot be neglected. The overall error is relatively high, but can be reduced with a better low-noise amplifier (LNA), thereby reducing $\Delta\overline{i^2_{D,F_m}}$. However, reduction of $\Delta\overline{i^2_{D,F_m}}$ in this manner will only be meaningful until the error becomes dominated by $\Delta\overline{i^2_{D,R_D/C_D}}$. In this case, other means to reduce the error become necessary, e.g., improvement in the measurement of the impedance elements through use of a more repeatable packaging technique.

V. Conclusion

We have proposed a technique to obtain the intrinsic circuit and noise elements of two-terminal devices using a two-port approach. The use of a full two-port S-parameter measurement allows us to extract the parasitic and intrinsic circuit elements with more precision than the reflection measurement which is usually used. The noise measurements with the noise-figure meter were performed by connecting the two-port in the same series configuration used for the S-parameter measurements. Precise knowledge of the equivalent-circuit elements is particularly important if the intrinsic noise is to be deembedded with reasonable accuracy. The error of the measured intrinsic data has been carefully evaluated and the error due to the equivalent-circuit elements was found to be significant and will become dominant when the error due to the noise measurement is lowered with a better preamplifier. The method is easily extended to higher frequencies and could also be used with a probe station, which will reduce the parasitics and lead to easier deembedding and, therefore, more accurate values for the intrinsic elements. As a demonstration of the technique, we have determined the element values of the impedance and noise equivalent circuit of an RTD.

Acknowledgment

The authors thank H. C. Liu and Z. R. Wasilewski, National Research Council of Canada, for providing the characterized RTD's. The authors further thank J. Kruger for fabricating the LNA, and H.-J. Ueng for assistance in developing the microwave deembedding software.

References

[1] A. Jelenski, A. Grüb, V. Krozer, and H. L. Hartnagel, "New approach to the design and the fabrication of THz Schottky barrier diodes," *IEEE Trans. Microwave Theory Tech.*, vol. 41, pp. 549–556, Apr. 1993.

[2] E. R. Brown, J. R. Söderström, C. D. Parker, L. J. Mahoney, K. M. Molvar, and T. C. McGill, "Oscillations up to 712 GHz in InAs/AlSb resonant tunneling diodes," *Appl. Phys. Lett.*, vol. 58, pp. 2291–2293, May 1991.

[3] J. M. M. Pantoja, A. Grüb, V. Krozer, and J. L. S. Franco, "Accuracy of nonoscillating one-port noise measurements," *IEEE Trans. Instrum. Meas.*, vol. 44, pp. 853–858, Aug. 1995.

[4] E. R. Brown, "High speed resonant tunneling diodes," in *Heterostructures and Quantum Devices* (VLSI Electronics: Microstructure Science Series, vol. 24), N. G. Einspruch and W. R. Frensely, Eds. New York: Academic, 1994, ch. 10, pp. 306–350.

[5] M. Trippe, G. Bosman, and A. van der Ziel, "Transit-time effects in the noise of Schottky-barrier diodes," *IEEE Trans. Microwave Theory Tech.*, vol. MTT-34, pp. 1183–1192, Nov. 1986.
[6] A. Jelenski, E. L. Kollberg, and H. H. G. Zirath, "Broad-band noise mechanisms and noise measurements of metal-semiconductor junctions," *IEEE Trans. Microwave Theory Tech.*, vol. MTT-34, pp. 1193–1201, Nov. 1986.
[7] W. C. B. Peatman and T. W. Crowe, "Design and fabrication of 0.5 micron GaAs Schottky barrier diodes for low-noise terahertz receiver applications," *Int. J. Infrared Millimeter Waves*, vol. 11, pp. 355–365, Mar. 1990.
[8] S. K. Diamond, E. Özbay, M. J. W. Rodwell, D. M. Bloom, Y. C. Pao, E. Wolak, and J. S. Harris, "Fabrication of 200-GHz $f_{\max}$ resonant-tunneling diodes for integrated circuit and microwave applications," *IEEE Electron Device Lett.*, vol. 10, pp. 104–106, Mar. 1989.
[9] G. F. Engen and C. A. Hoer, "Thru-reflect-line: An improved technique for calibrating the dual six-port automatic network analyzer," *IEEE Trans. Microwave Theory Tech.*, vol. MTT-25, pp. 987–993, Dec 1979.
[10] G. Dambrine, A. Cappy, F. Heliodore, and E. Playez, "A new method for determining the FET small-signal equivalent circuit," *IEEE Trans. Microwave Theory Tech.*, vol. 36, pp. 1151–1159, July 1988.
[11] D. F. Wait, "Thermal noise from a passive linear multiport," *IEEE Trans. Microwave Theory Tech.*, vol. MTT-16, pp. 687–691, Sept. 1968.
[12] G. Martines and M. Sannio, "The determination of the noise, gain and scattering parameters of microwave transistors (HEMT's) using only an automatic noise figure test-set," *IEEE Trans. Microwave Theory Tech.*, vol. 42, pp. 1105–1113, July 1994.
[13] A. Przadka, K. J. Webb, D. B. Janes, H. C. Liu, and Z. R. Wasilewski, "Microwave measurement of shot noise in resonant tunneling diodes," *Appl. Phys. Lett.*, vol. 71, pp. 530–532, July 1997.

Andreas Przadka received the Dipl. Ing. degree from Ruhr-Universitat-Bochum, Germany, in 1995, and is currently working toward the Ph.D. degree at Purdue University, West Lafayette, IN.

His research interests include fabrication, measurement, and modeling of microwave devices and vertical high-power microwave devices in silicon carbide.

Kevin J. Webb (S'81–M'84-SM'98) received the B.Eng. and M.Eng. degrees from the Royal Melbourne Institute of Technology, Melbourne, Australia, in 1978 and 1981, respectively, the MSEE degree from the University of California at Santa Barbara, in 1981, and the Ph.D. degree from the University of Illinois at Urbana-Champaign, in 1984.

After spending five years as a Faculty Member at the University of Maryland at College Park, he joined the School of Electrical and Computer Engineering, Purdue University, West Lafayette, IN, in 1990.

David B. Janes (S'86–M'89) was born in Somerset, KY, in 1958. He received the B.A. degree in physics (*summa cum laude*) from Augustana College, Rock Island, IL, in 1980, and the B.S.E.E. (highest honors), M.S.E.E. and Ph.D. degrees from the University of Illinois at Urbana-Champaign, in 1980, 1981, and 1989, respectively.

From 1981 to 1985, he was a Research Scientist in the Research Division, Raytheon Company, where he was involved in research on microwave semiconductor devices, including GaAs IMPATT diodes and MESFET's and monolithic microwave integrated circuits. Since 1989, he has been with the School of Electrical and Computer Engineering, Purdue University, West Lafayette, IN, where he is currently a Principal Research Engineer. He is currently engaged in experimental research on mesoscopic semiconductor devices and nanoscale metallic cluster arrays, characterization of novel semiconductor heterostructures, and microwave devices based on compound semiconductor heterostructures.